K_1 (373 K) = (3.3 ± 0.4) × 10^3; K_1 (393 K) = (1.1 ± 0.2) × 10^3).

Kinetic experiments were performed over a range of conditions (P_{CH_4} = 1-10 atm; $[CH_4]$ = (2.4-24) × 10^{-2} M; T = 296-393 K; [(TMP)Rh•] = (6-9) × 10^{-4} M). The methane concentration in solution and the reservoir of methane gas are large compared to the [(TMP)Rh•], which ensures that the observed kinetics for a single sample is pseudo zero order in methane. When the methane concentration is large ($P_{CH_4} \approx 10$ atm) and the temperature relatively low (T = 296 K), reaction 1 proceeds to virtual completion. Plots of $[(TMP)Rh•]^{-1}$ versus time are linear for more than 3 half-lives, which clearly indicates that reaction 1 is second order in [(TMP)Rh•] ($rate_{f(1)} = -d[(TMP)Rh•]/2dt = k'[(TMP)Rh•]^2$). Variation of the methane concentration was used in determining that reaction 1 is first order in methane ($rate_{f(1)} = k[(TMP)Rh•]^2[CH_4]$). Final analysis of the kinetic data was obtained by simulating the concentration versus time profiles by treating reaction 1 as a third-order process approaching equilibrium and using the experimentally determined equilibrium constants. Simulation of the concentration versus time profiles was obtained by use of the computer program GEAR adapted by T. E. Beukelman and F. G. Weigert from HAVCHM, written by R. N. Stabler and J. Chesick (*Int. J. Chem. Kinet.* **1978**, *10*, 461-469). The PC version (1.1) was converted to Microsoft Fortran (v. 3.31) by R. J. McKinney.

(TMP)Rh• with $CH_3C_6H_5$ and $CD_3C_6D_5$. Stock solutions of $CH_3C_6H_5$ and $CD_3C_6D_5$ (0.100 M) in benzene were prepared in an inert atmosphere box, placed in a vacuum transfer tube, degassed, and stored under argon. Weighed samples of (TMP)Rh-CH_3 were placed into vacuum-adapted NMR tubes, dissolved in benzene, and irradiated in a Rayonnet photoreactor for 6 h (λ ≥ 350 nm) to form (TMP)Rh•. The solvent was then pumped off and 0.5 mL of the toluene stock solution syringed in under argon. The NMR tubes were then attached to a vacuum line and subjected to three freeze-pump-thaw cycles and sealed under vacuum. The samples were subsequently heated in a constant-temperature oil bath, and the concentration of the constituents was periodically monitored by ^{1}H NMR. Linearity of plots for $[(TMP)Rh•]^{-1}$ versus time and variation of the toluene concentration indicate that the rate law for reaction 5 is second order in [(TMP)Rh•] and first order in toluene ($rate_{f(5)} = k_5[(TMP)Rh•]^2[CH_3C_6H_5]$).

[(TXP)Rh]$_2$ with CH_4. Relative concentrations of $[(TXP)Rh]_2$, (TXP)Rh-H, and (TXP)Rh-CH_3 were determined by using ^{1}H NMR by comparing the integrated intensities of the pyrrole H resonances of metastable C_6D_6 solutions at 296 K. Three sequential recordings of the spectra demonstrated that the ratio of concentrations remained constant during the time required for data acquisition. Absolute concentrations were obtained by using methane as an internal standard. Kinetic experiments were performed at methane pressures ($P_{CH_4} \approx 1$-6 atm; $[CH_4] \approx (0.24\text{-}1.4) \times 10^{-1}$ M) such that reaction 2 is pseudo zero order in CH_4. Reaction 2 achieves an observable equilibrium position at each of the conditions studied. Equilibrium constants for reaction 2 were evaluated by integration of ^{1}H NMR at equilibrium (K_2 (353 K) = 0.03 ± 0.01; K_2 (393 K) = 0.04 ± 0.01). The combination of experimental error and the complexity associated with a process that achieves observable equilibrium reduces the clarity of defining the rate law. Rate data for reaction 2 are satisfactorily fitted to a process that is first order in both $[(TXP)Rh]_2$ and CH_4 that proceeds to equilibrium, but this description may not be unique. Representative kinetic studies at 1.40 and 5.20 atm of CH_4 illustrate that the rate for reaction 2 can be described as first order in methane at T = 353 K (P_{CH_4} = 1.40 atm, $[CH_4] = 3.55 \times 10^{-2}$ mol L^{-1}, $[(TXP)Rh]_2 = 6.30 \times 10^{-4}$ mol L^{-1}, $k_2' = 1.68 \times 10^{-5}$ s^{-1}, k_2 (353 K) = 4.72 × 10^{-4} mol L^{-1} s^{-1}; P_{CH_4} = 5.18 atm, $[CH_4]$ = 0.1270 mol L^{-1}, $[(TXP)Rh]_2 = 4.48 \times 10^{-4}$ mol L^{-1}, $k_2' = 5.64 \times 10^{-5}$ s^{-1}, k_2 (353 K) = 4.44 × 10^{-4} L mol^{-1} s^{-1}). The best fit for the data in Figure 5 for reaction 2 occurring by a process that is first order in both $[(TXP)Rh]_2$ and CH_4 and approaching equilibrium is found for the following rate and equilibrium constants: k_2 (353 K) = 0.44 × 10^{-3} L mol^{-1} s^{-1}, K_2 (353 K) = 0.034; k_2 (393 K) = 6.1 × 10^{-3} L mol^{-1} s^{-1}, K_2 (393 K) = 0.028. The equilibrium constants from analysis of the kinetic data (K_2 (353 K) = 0.034; K_2 (393 K) = 0.028) are in reasonable agreement with the values from integration of ^{1}H NMR at equilibrium (K_2 (353 K) = 0.04 ± 0.01; K_2 (393 K) = 0.03 ± 0.01). The best fit was obtained by using the computer program GIT, written by F. J. Weigert and modified by T. E. Beukelman from HAVCHM (*Int. J. Chem. Kinet.* **1978**, *10*, 461-469).

Acknowledgment. We gratefully acknowledge support of this work by the National Science Foundation through Grant CHE-9014923.

1*H*-Bicyclo[3.1.0]hexa-3,5-dien-2-one. A Strained 1,3-Bridged Cyclopropene

Wolfram Sander,*,† Götz Bucher,† Felix Reichel,‡ and Dieter Cremer*,‡

Contribution from the Institut für Organische Chemie der Technischen Universität, Hagenring 30, D-3300 Braunschweig, FRG, and Department of Theoretical Chemistry, University of Göteborg, Kemigarden 3, S-41296 Göteborg, Sweden. *Received November 27, 1990. Revised Manuscript Received February 19, 1991*

Abstract: Triplet 4-oxocyclohexa-2,5-dienylidene (**5**) gives 1*H*-bicyclo[3.1.0]hexa-3,5-dien-2-one (**4**) on irradiation into its long-wavelength triplet-triplet absorption band (λ = 508-566 nm). Bicyclus **4** was characterized by IR spectroscopy in partially oriented matrices, by deuterium and oxygen-18 isotopic labeling and by comparison of experimental data with ab initio calculations. **4** is highly labile and readily rearranges back to carbene **5** thermally or on visible light (λ = 470 nm) or infrared irradiation. The rates of the thermal **4** → **5** rearrangement have been measured in argon, krypton, xenon, and nitrogen matrices, and deuterium kinetic isotope effects have been determined. The data show that **4** is directly transformed into **5**, with intersystem crossing being rate determining. At low temperatures (<20 K), the rates are independent of temperature, which indicates that the rearrangement occurs via quantum mechanical tunneling. MP2/6-31G(d) calculations show that the cyclopropene ring in **4** is tilted by 129.6° with regard to the cyclopentene ring. The torsional angle between the two carbon 2pπ-orbitals in the cyclopropene ring is 9°, and the pyramidalization angles at C5 are 19.2°. The extra strain energy caused by distortion of the cyclopropene double bond is compensated by the π-stabilization energy of the dienone system. Thus, the total strain energy is only 54 ± 1 kcal/mol—comparable to the strain energy of cyclopropene.

1,3-Bridged cyclopropenes **1** are unstable and highly reactive if the bridge is smaller than n = 6.[1a]

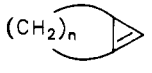

1

While bicyclo[5.1.0]octene (n = 5) slowly dimerizes at room temperature via an ene reaction, bicyclo[4.1.0]heptene (n = 4) is only stable at temperatures below -90 °C. Bicyclo[3.1.0]hexene (n = 3) (**2a**) (Scheme I) has not yet been characterized by spectroscopic methods, but some of its derivatives (**2b-e**) have been trapped in solution.[1]

†Technische Universität Braunschweig.
‡University of Göteborg.

(1) (a) Billups, W. E.; Haley, M. M.; Lee, G.-A. *Chem. Rev.* **1989**, *89*, 1147. (b) Halton, B.; Bridle, J. H.; Lovett, E. G. *Tetrahedron Lett.* **1990**, *31*, 1313.

0002-7863/91/1513-5311$02.50/0

Table I. IR Spectroscopic Data of Carbene **5** Matrix-Isolated in Ar at 10 K and Data Calculated by ab Initio Methods (UHF/6-31G(d))

Ar matrix				UHF/6-31G(d)				
ν (cm^{-1})	I^a	Δ^b	DCR^c	ν (cm^{-1})^d	I^a	Δ^b	diff^e	assignment^f
2966.0	11.1							2 × 1496.5
2953.0	2.1		0.781	2972.9	0.0	0.740	19.9	C-H str
2950.6	2.1		0.779	2971.9	18.3	0.740	21.3	C-H str
2865.2	2.5		0.791	2956.3	7.4	0.738	91.1	C-H str
2848.8	1.3		0.793	2955.8	6.1	0.737	107.0	C-H str
1872.5	4.5							2 × 937.7
1506.1	29.6	0.97						
1497.9	91.6							C=O str
1496.5	100.0	0.89	0.994	1245.9	37.1	1.008	-250.6	
1482.0	19.4	0.85	0.976	1373.0	34.2	0.955	-109.0	C=C ip
1464.7	15.4	1.19	0.977	1394.3	20.2	0.968	-70.4	skel ip
1375.5	33.3	0.91	0.891	1360.5	0.5	0.857	-15.0	C-H ip
1362.5	15.5	1.18	0.953	1282.9	1.4	0.956	-79.6	skel ip
1260.3	36.3	1.15	1.000	1223.2	21.2	0.965	-37.1	C-H ip
1248.2	8.4	1.18	0.991	1201.1	8.3	0.789	-47.1	C-H ip
1076.6	22.4	1.16	0.914	1005.6	3.4	0.755	-71.0	C-H
937.7	25.4	0.85	0.991	919.0	2.2	0.732	-18.7	C-H oop
819.1	97.1	0.93	0.862	738.1	100.0	0.857	-81.0	C-H oop

^{a} Relative intensity. ^{b} Ratio of isotopic frequencies ν^i/ν for [d_4]**5** and **5**. ^{c} Dichroic ratios I_z/I_y in a typical experiment. ^{d} Calculated frequencies have been scaled by a factor of 0.87. ^{e} Deviation of the calculated from experimental frequencies. ^{f} ip = in-plane; oop = out-of-plane.

Scheme I

2 3

X-Y-Z		X-Y-Z	
a	-CH_2-CH_2-CH_2-	d	-$Si(CH_3)_2$-CH_2-CH_2-
b	-CH_2-O-CH_2-	e	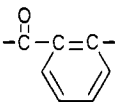
c	-CH_2-S-CH_2-		

The experiments in solution show that the cyclopropene ring in **2** readily opens to give cyclohexenylidene (**3**). The equilibrium between **2** and **3** depends on the length of the X–Y–Z chain (Scheme I). Heteroatoms with relatively short bond lengths (O in **2b**) destabilize, while heteroatoms with long bond lengths (Si in **3d**) stabilize the bicyclic system **2**.

In this paper, we describe the first spectroscopic characterization of a compound with the bicyclo[3.1.0]hex-5-ene skeleton. 1*H*-Bicyclo[3.1.0]hexa-3,5-dien-2-one (**4**) is only metastable even at 10 K and easily rearranges to triplet 4-oxocyclohexa-2,5-dienylidene (**5**). Several aspects of the chemistry of **4** mimic properties of singlet carbenes.[2]

4-Oxocyclohexa-2,5-dienylidene (5)

The photoelimination of nitrogen from quinonediazides is of technical importance for photolithography and has thus been studied fairly well.[3] Carbene **5** and many of its derivatives have been produced in solution by photolysis[4] or thermolysis[5] of the corresponding diazo compounds. In most cases, the addition of **5** to olefins is stereospecific and in the reaction with methanol O–H insertion is preferred over C–H insertion.[3] This chemistry is in accordance with reaction from the singlet state. On the other hand, H abstractions[4a,6] and the induction of polymerizations are also known, which is typical of triplet reactivity. Thus, carbene **5** in solution exhibits both singlet and triplet reactivity, and the course of its reactions depends much on experimental conditions.

Table II. UV–Vis Data of **5** and [d_4]**5** Matrix-Isolated in Ar at 10 K

5, λ_{max} (nm)	[d_4]**5**, λ_{max} (nm)	polzn^a
566 (w)	566 (w)	*Z*
550 (w)	550 (w)	*Z*
535 (w)	536 (w)	*Z*
521 (w)	524 (w)	*Z*
508 (w)	512 (w)	*Z*
496 (w)		*Z*
379 (m)	380 (m)	*Y*
367 (m)	368 (m)	*Y*
351 (m)	352 (m)	*Z*
338 (m)	338 (m)	*Z*
297 (s)	298 (s)	
290 (s)	290 (s)	
	242 (s)	

^{a} Polarization direction determined after irradiation with *Z*-polarized light.

At low temperature, it is possible to determine the lowest spin state of **5**. In an ESR study, Wasserman and Murray generated **5** by irradiation of powder samples of **6** at 4 K with UV light and could prove the triplet ground state of this carbene.[7] The electronic structure of **5** (if no spin state is specified, **5** means the triplet ground state; otherwise, T-**5** and S-**5** mean the lowest triplet and singlet state, respectively) resembles that of a phenoxyl radical for the π-system—as indicated by the low *D* value of 0.3179 cm^{-1} for **5**[2a,7]—and a phenyl radical for the σ-system. A spin density of 0.4 is estimated for the π-system at C1 from the ESR data.

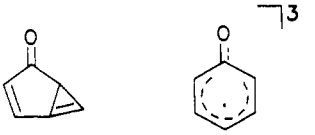

4 T-5

Spectroscopic Characterization of 5. Here we describe matrix isolation studies on **5** and several of its isotopomers. Quinone-

(2) (a) Sander, W.; Mueller, W.; Sustmann, R. *Angew. Chem.* **1988**, *100*, 577; *Angew. Chem., Int. Ed. Engl. 27*, 572. (b) Sander, W. W.; Patyk, A.; Bucher, G. *J. Mol. Struct.* **1990**, *222*, 21.

(3) Ershov, V. V.; Nikiforov, G. A.; de Jonge, C. R. *Quinonediazides*; Elsevier: Amsterdam, 1981.

(4) (a) Vorotnikov, A. P.; Davydov, E. Y.; Toptygin, D. Y. *Izv. Akad. Nauk SSSR, Ser. Khim.* **1985**, 1275. (b) Sundberg, R. J.; Baxter, E. W. *Tetrahedron Lett.* **1986**, *27*, 2687.

(5) (a) Plekhanova, L. G.; Nikiforov, G. A.; Ershov, V. V.; Zakharov, E. P. *Izv. Akad. Nauk SSSR, Ser. Khim.* **1973**, 846. (b) Nikiforov, G. A.; Markaryan, S. A.; Plekhanova, L. G.; Sviridov, B. D.; Pehk, T.; Lipmaa, E.; Ershov, V. V. *Izv. Akad. Nauk SSSR, Ser. Khim.* **1974**, 93. (c) Nikiforov, G. A.; Sviridov, B. D.; Ershov, V. V. *Izv. Akad. Nauk SSSR, Ser. Khim.* **1974**, 373. (d) Plekhanova, L. G.; De Jonge, C. R. H. I.; Nikiforov, G. A.; Ershov, V. V. *Izv. Akad. Nauk SSSR, Ser. Khim.* **1979**, 409. (e) Plekhanova, L. G.; Nikiforov, G. A.; De Yonge, C. *Izv. Akad. Nauk SSSR, Ser. Khim.* **1980**, 136.

(6) Korshak, V. V.; Vorotnikov, A. P.; Davydov, E. Y.; Kozyreva, N. M.; Kirilin, A. I.; Skubina, S. B.; Toptygin, D. Y. *Dokl. Akad. Nauk SSSR* **1986**, *291*, 376.

(7) Wasserman, E.; Murray, R. W. *J. Am. Chem. Soc.* **1964**, *86*, 4203.

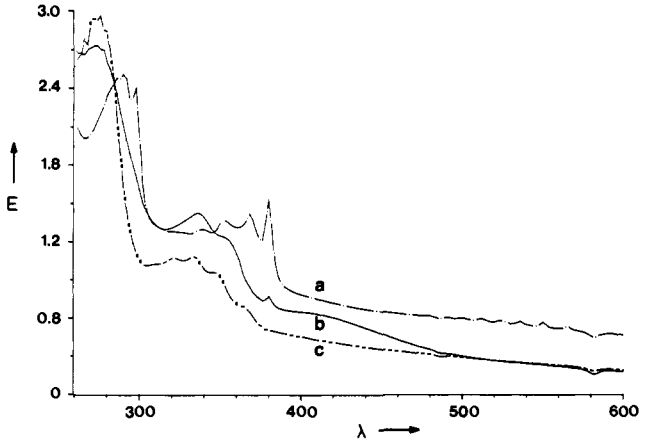

Figure 1. UV-vis spectra of 5 (a), 4 (b), and 14a (c).

Table III. Some Geometric Parameters and Dipole Moment of Carbene 5, Calculated by ab Initio Methods[a]

	UHF/3-21G	UHF/6-31G(d)
C1–C2	1.395	1.399
C2–C3	1.392	1.390
C3–C4	1.428	1.445
C4–O	1.305	1.251
C2–H	1.071	1.074
C3–H	1.070	1.074
C1–C2–C3	117.6	117.6
C2–C3–C4	120.5	120.3
C3–C4–O	120.4	120.5
μ	1.997	2.343
$\langle S^2 \rangle$[b]	2.77	2.70

[a] Bond length in angstroms, bond angle in degrees, dipole moment in debye. [b] Expectation value of $\langle S^2 \rangle$ from UHF calculations.

diazide 6, its tetradeuterated isotopomer [d_4]6, and the ^{18}O-labeled isotopomer [^{18}O]6 have been isolated in argon, krypton, xenon, and nitrogen matrices. If matrix-isolated 6 was irradiated ($\lambda >$ 495 nm) at 10 K, carbene 5 was formed rapidly as the major photoproduct. Irradiation using grey filters reveals that the formation of 5 linearly depends on the intensity of light, and Lambert–Beer's law is obeyed. A minor photoproduct is the photoisomer of 5 (see below). Carbene 5 has been identified by IR (Table I), UV (Figure 1 and Table II), and ESR spectroscopy[2a] as well as through its reactions with CO[2a] and O_2.[9]

The ESR spectrum of matrix-isolated 5[2a] is basically identical with the spectrum reported by Wasserman and Murray,[7] which proves that the same species is obtained in the powder sample and in the matrix. Between 23 and 45 K, the Curie law is obeyed and thus 5 has a triplet ground state.[2a] The matrix IR spectrum shows a strong peak at 1496.5 cm^{-1} that exhibits an isotopic shift of only −8.7 cm^{-1} in [d_4]5 but −28.5 cm^{-1} in [^{18}O]5 and is assigned to the C–O stretching vibration. This low-frequency vibration implies a bond order of approximately 1.5 for the C–O bond. A second strong peak at 819.9 cm^{-1} exhibits a deuterium isotopic shift of −112.8 cm^{-1} and is assigned to an out-of-plane C–H deformation mode. Partially aligned matrices have been produced by photoselection with linearly polarized light to allow the assignment of IR bands of 5 and [d_4]5. These experiments are described below.

Ab initio calculations at the UHF/6-31G(d) level have been performed (Figure 7, Table III). According to these calculations, 5 has a planar structure with C_{2v} symmetry. One of the unpaired electrons is localized at C1; the other is delocalized in the π-system. As a result of this delocalization, the C–O bond length is longer than expected for a double bond and the C1–C2 and C2–C3 bond lengths are almost identical (Figure 7, Table III). The IR spectrum is reproduced only poorly at the UHF/6-31G(d) level of theory. The C–O stretching mode is calculated at 1245.9 cm^{-1} if a scaling factor of 0.875 is used (this scaling factor gives an excellent fit of experimental and calculated IR data for 4; see below), indicating that delocalization is overestimated by the calculation. Similar observations have been made when investigating conjugated cyclic systems at the UHF level of theory.

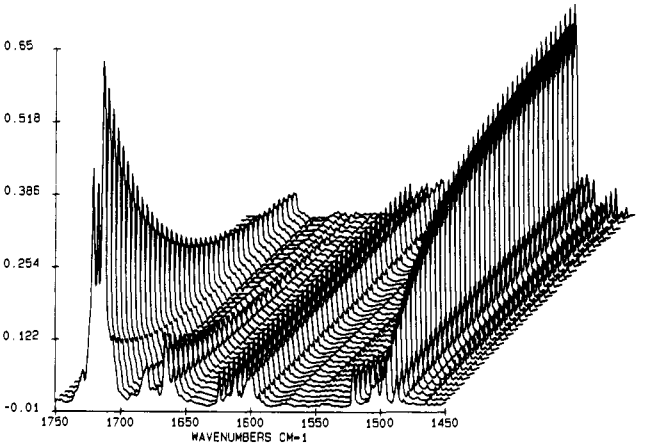

Figure 2. Carbonyl region of IR spectra showing the infrared-induced isomerization of 4 (front) to 5 (back).

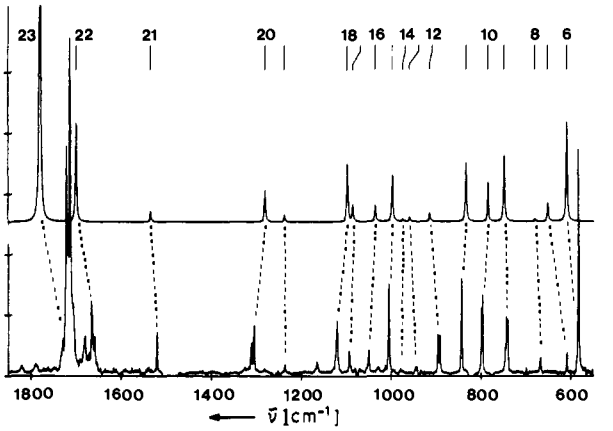

Figure 3. IR spectra of 4 matrix-isolated in Ar at 10 K (bottom, difference spectrum showing peaks assigned to 4) and calculated with the RHF/6-31G(d) basis set (top). The numbers refer to Table IV.

The carbene was further characterized by its chemistry. A reaction typical for triplet carbenes is the rapid addition of $^3O_2$ to give carbonyl *O*-oxides.[8] The thermal reaction of matrix-isolated 5 with $^3O_2$ leads to high yields of *p*-benzoquinone *O*-oxide, which has been described elsewhere.[9] Another important reaction for free carbenes in matrices is the thermal reaction with CO to give ketenes.[10] Warming of 5, matrix-isolated in Ar doped with 1% CO, from 10 to 35 K (softening temperature of the argon matrix) resulted in a decrease of 5 and formation of a new compound. On the basis of its IR spectrum (Ar, 10 K; 2110 (s), 1635 (s), 1158 (m), 851 (m), 707 (m) cm^{-1}), which shows absorptions typical for both ketene and ketone functional groups, this compound was assigned to ketoketene 7.

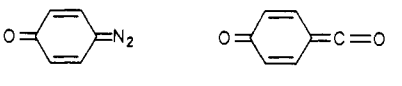

6 7

Photoisomerization of 5. Carbene 5 proved to be photolabile on irradiation (543 nm) into the long-wavelength triplet–triplet absorption band (Figure 1). The conversion to a photoproduct (A) proceeds to >90% after several hours of irradiation; prolonged irradiation leads neither to complete conversion nor to the formation of further products.[11] The photoisomerization is com-

(8) Sander, W. *Angew. Chem.* **1990**, *102*, 362; *Angew. Chem., Int. Ed. Engl.* *29*, 344.
(9) Sander, W. W. *J. Org. Chem.* **1988**, *53*, 2091.
(10) Baird, M. S.; Dunkin, I. R.; Hacker, N.; Poliakoff, M.; Turner, J. J. *J. Am. Chem. Soc.* **1981**, *103*, 5190.

Table IV. IR Spectroscopic Data of **4** Matrix-Isolated in Ar at 10 K and IR Spectrum Calculated by ab Initio Methods (RHF/6-31G(d))

	Ar matrix					RHF/6-31G(d)					
Nr	ν (cm^{-1})	I^a	DCR[b]	Δ^c	Δ^d	ν (cm^{-1})[e]	I^a	Δ^c	Δ^d	diff[f]	assignment[g]
27	3084.6	2.5	0.74			3036.9	0.2	0.753	1.000	−47.71	C–H str
26	3022.4	2	0.75			3004.1	2.6	0.746	1.000	−18.27	C–H str
25	3012.7	1	0.75			2983.9	0.5	0.738	1.000	−28.76	C–H str
24	3008.4	2.2				2880.3	7.9	0.737	1.000		C–H str
23	1720.7	69.1	1.18								C=O str
	1713.4	100.0	1.16	0.996	0.986	1778.2	100.0	0.998	0.981	64.79	
	1680.2	11.7	1.15	0.983	0.994						$2 \times \nu_{11}$
22	1665.2	21.5	1.54	0.975	0.998	1698.2	18.8	0.968	0.999	32.96	C=C str (3 ring)
21	1520.6	12.2	1.11	0.970	0.999	1532.6	2.1	0.968	1.000	11.99	C=C str (5 ring)
20	1305.6	14.2	1.45	0.886	1.001	1279.1	6.1	0.886	1.000	−26.54	
19	1236.6	2.3	0.57	0.886	0.999	1236.0	1.4	0.895	1.000	−0.60	
	1165.8	3.3	0.69		0.998						$2 \times \nu_6$
18	1121.4	14.2	0.88	0.921	0.998	1095.9	11.1	0.931	0.999	−25.46	
17	1094.4	6.8	0.65	0.839	0.997	1083.7	3.2	0.840	1.000	−10.65	
16	1050.5	7.9	1.49	0.787	1.000	1033.7	3.1	0.817	1.000	−16.81	
15	1005.7	26.9	0.67	0.872	0.999	996.3	8.9	0.858	1.000	−9.37	
14	979.7	1.6		0.833	0.997	972.6	0.5	0.836	1.000	−7.08	
13	943.0	2.6	1.02	0.812	1.002	958.0	0.9	0.790	1.000	15.02	
12	896.7	11.9	1.19	0.866	1.000	913.3	1.7	0.857	1.000	16.62	
11	843.2	29.4	1.39	0.877	0.998	832.4	11.3	0.890	0.999	−10.83	
10	796.9	24.5	0.55	0.857	1.001	783.4	7.5	0.865	0.999	−13.49	
9	741.0	16.5	0.91	0.815	1.003	747.4	12.7	0.813	1.000	6.38	
8	669.2	5.5	0.59	0.942	0.996	679.9	0.5	0.962	0.998	10.67	
7	608.9	6.5	0.81	0.896	0.997	649.8	3.5	0.910	1.000	40.95	
6	583.4	69.7	0.65	0.843	0.999	608.1	19.1	0.842	0.999	24.70	

[a] Relative intensity. [b] Dichroic ratios I_z/I_y in a typical experiment. [c] Ratio of isotopic frequencies ν^i/ν for [d_4]**4** and **4**. [d] Ratio of isotopic frequencies ν^i/ν for [^{18}O]**4** and **4**. [e] Calculated frequencies have been scaled with 0.87. [f] Deviation of the calculated from experimental frequencies. [g] Due to the low symmetry of **4**, only approximate description. The low-frequency modes have contributions from many atoms, and therefore a description is not given.

Table V. UV–Vis Data of **4** and **14a** Matrix-Isolated at 10 K

4 (Ar matrix), λ_{max} (nm)	**4** (Xe matrix), λ_{max} (nm)	polzn[a]	**4** (CNDO/S), λ (nm)	log ϵ	z	y	x[b]	**14a** (Ar matrix), λ_{max} (nm)
418 (br)	398 (br)	Z	432	3.02	−0.2	−1.2	0.5	
356 (m)	354 (sh)	Z	372	3.08	−0.1	−1.3	0.3	368 (sh)
								348 (sh)
								334 (m)
342 (m)	342 (m)	Z	331	2.69	0.1	0.6	0.4	322 (m)
272 (s)	282 (sh)		290	3.47	−0.5	−0.4	1.7	252 (s)
232 (s)			237	3.28	0.1	−0.1	−1.3	216 (s)

[a] Polarization direction determined after irradiation with Z-polarized light. [b] Components of the calculated transition moment.

pletely reversible (>99%) on slightly shorter wavelength irradiation ($\lambda > 495$ nm). Obviously on 543 nm irradiation a photostationary equilibrium of **5** and the photoisomer A is achieved. The back-isomerization is also induced by IR irradiation (Figure 2) and thermally (for a discussion, see Kinetics). The thermal back-reaction proves that the photoisomer A is higher in energy than carbene **5**.

From the absence of an ESR signal, we conclude that A has a singlet ground state. A strong peak at 1713.4 cm^{-1} in the IR (Figures 2, 3, and 8, Table IV), which exhibits an ^{18}O isotopic shift of −24.1 cm^{-1} and a deuterium shift of −6.7 cm^{-1} (on per-deuteration), indicates the presence of a carbonyl group. Possible structures for A, which have to be considered, are presented in Scheme II. The singlet carbene **S-5** and the bicyclic compounds **4** and **8** have the same C–H connectivity as **T-5**, and their formation does not require H shifts. For cyclopropanone **8**, a strong carbonyl band above 1800 cm^{-1} and an absorption of the allene substructure around 1900 cm^{-1} are expected. From the absence of absorptions between 1750 and 3000 cm^{-1}, structure **8** can be excluded and only **S-5** and **4** are considered further.

The compounds on the right-hand side of Scheme II can only be formed if a formal H shift (1,2 or 1,3) is involved in the rearrangement. From the absence of strong deuterium effects on kinetics, we conclude that a H shift is not involved in the rate-determining step (see below). Wolff rearrangement of

Scheme II

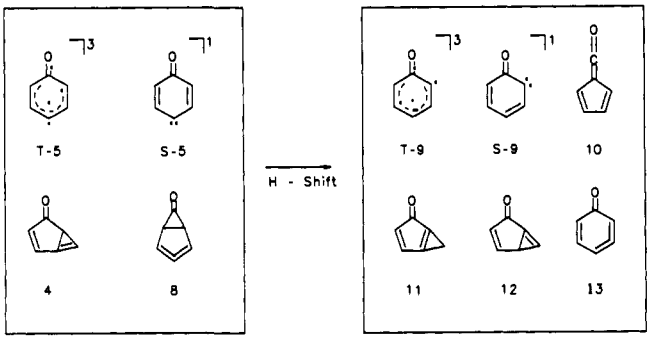

carbene **9** to ketene **10** is fast, even under the conditions of matrix isolation.[10,12] Ketene **10** is not formed in the matrix, and therefore **9**—and also **12**, which is expected to ring open to **9**—is excluded as a possible structure for A.

1*H*-Bicyclo[3.1.0]hexa-3,5-dien-2-one (4)

A positive identification of **4** as the photoproduct of **5** comes from comparison of its IR and UV–vis spectra with bicyclo-[3.1.0]hex-3-en-2-one (**14a**), by comparison of the IR spectrum with high-level ab initio calculations, and by measuring IR dichroism of partially aligned matrices.

(11) Short-wavelength irradiation ($\lambda < 400$ nm) leads to the formation of a ring-opened compound with a ketene and terminal acetylene functional group of unknown structure (ref 2a).

(12) McMahon, R. J.; Chapman, O. L.; Hayes, R. A.; Hess, T. C.; Krimmer, H. P. *J. Am. Chem. Soc.* **1985**, *107*, 7597.

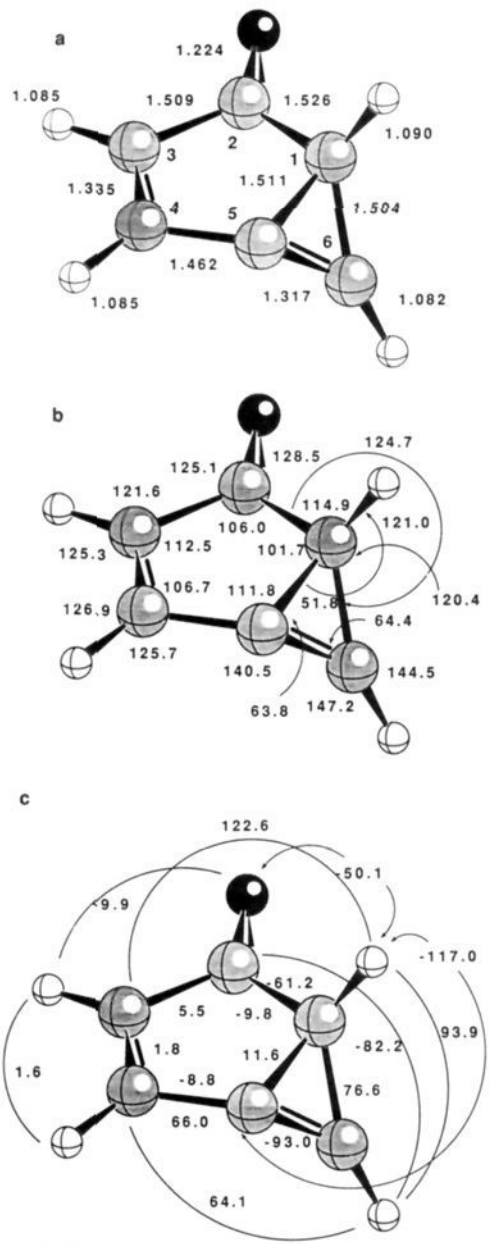

Figure 4. MP2/6-31G(d) structure of **4**: (a) bond lengths, (b) bond angles, (c) dihedral angles.

Geometry and IR spectrum of **4** have been calculated both at the RHF/3-21G[13a] and at the RHF/6-31G(d)[13b] level of theory. Some of these results are listed in Tables IV and VI. In addition to the RHF calculations, a complete geometry optimization of **4** has also been carried out at the RMP2/6-31G(d) level of theory[14] in order to get a reliable description of the electronic structure of **4** and to determine strain energy and heats of formation of the bicyclus. MP2 geometrical data are summarized in Figure 4 and Table VI. Finally, the UV–vis spectrum of **4** has been investigated with CNDO/S[15] by utilizing the RMP2/6-31G(d) geometry (Table V).

Geometry of 4. The five-membered ring is slightly puckered, with C1 being shifted out of the almost perfect plane defined by C2, C3, C4, C5, and O; i.e. the ring adopts a C1 envelope form with a puckering amplitude of 0.11 Å and a phase angle (7.95°)

Table VI. Some Geometric Parameters of **4** Calculated by ab Initio Methods

	RHF/3-21G	RHF/6-31G(d)	MP2/6-31G(d)	model comp
C1–C2	1.528	1.528	1.526	1.495[a]
C1–C5	1.502	1.483	1.511	1.498[a]
C1–C6	1.531	1.501	1.504	1.516[a]
C2–O	1.205	1.187	1.225	1.217[a]
C2–C3	1.529	1.521	1.509	1.477[a]
C3–C4	1.329	1.330	1.355	1.335[a]
C4–C5	1.477	1.483	1.462	1.477[a]
C5–C6	1.291	1.283	1.317	1.300[b]
C2–C1–C5	101.7	101.3	101.7	
C2–C1–C6	121.5	124.2	124.7	
C1–C6–C5	63.7	63.8	64.4	
C1–C5–C6	66.0	65.3	65.3	
C2–C3–C4	113.0	112.5	112.5	
C3–C4–C5	106.65	106.4	106.8	
O–C2–C1–C6	123.1	123.8	126.2	
O–C2–C3–C4	−179.0	−179.7	−178.5	

[a] (*R,S*)-6-*exo*-Acetoxy-3,6-dimethylbicyclo[3.1.0]hex-3-en-2-one (**14b**), X-ray data, ref 17. [b] Cyclopropene, microwave data, ref 18.

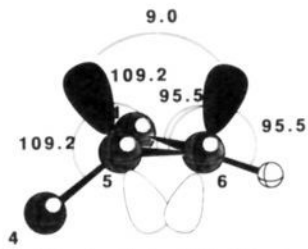

Figure 5. Distortion of the double bond C5–C6 and pyramidalization at C5 and C6 in the bicyclic compound **4**.

close to 0° that defines an exact envelope form.[16] The cyclopropene ring is tilted by 129.6° with regard to the cyclopentene ring. Calculated bond lengths in the cyclopentenone part of the molecule are similar to those determined in an X-ray structure of (*R,S*)-6-*exo*-acetoxy-3,6-dimethylbicyclo[3.1.0]hex-3-en-2-one (**14b**)[17] (Table VI). Also, the calculated double bond length C5–C6 does not possess an exceptional value, being 1.317 Å slightly longer than the corresponding bond length in cyclopropene (1.300 Å[18]).

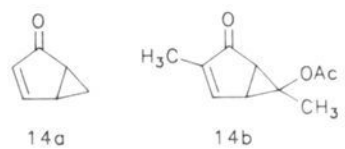

14a 14b

Electronic Structure of 4. The incorporation of a double bond into the three-membered ring of a bicyclus is known to lead to a dramatic increase of the strain energy. For example, the strain energy increases by 65 kcal/mol when going from bicyclo[2.1.0]pentane to bicyclo[2.1.0]pent-1(5)-ene.[19]

Since the double bond in the three-membered ring of a bicyclus such as **4** becomes strongly distorted, one could expect a (partial) decoupling of the π-electron pair and the possibility of a low-lying triplet state. This possibility was ruled out by calculating the lowest lying triplet at UMP2/6-31G(d) by utilizing the corresponding RMP2 geometry. Its relative energy (104 kcal/mol)

(13) (a) Binkley, J. S.; Pople, J. A.; Hehre, W. J. *J. Am. Chem. Soc.* **1980**, *102*, 939. (b) Hariharan, P. C.; Pople, J. A. *Theor. Chim. Acta* **1973**, *28*, 213.
(14) Pople, J. A.; Krishnan, R.; Schlegel, H. B.; Binkley, J. S. *Int. J. Quantum Chem.* **1979**, *13*, 225.
(15) (a) Del Bene, J.; Jaffé, H. H. *J. Chem. Phys.* **1968**, *48*, 1807. (b) Baumann, H. F. *QCPE 333*; Bloomington, IN, 1975.
(16) (a) Cremer, D.; Pople, J. A. *J. Am. Chem. Soc.* **1975**, *97*, 1354. (b) Cremer, D. *J. Phys. Chem.* **1990**, *94*, 5502.
(17) Quinkert, G.; Kleiner, E.; Freitag, B.-J.; Glenneberg, J.; Billhardt, U.-M.; Cech, F.; Schmieder, K. R.; Schudok, C.; Steinmetzer, H.-C.; Bats, J. W.; Zimmermann, G.; Dürner, G.; Rehm, D. *Helv. Chim. Acta* **1986**, *69*, 469.
(18) Kasai, P. H.; Myers, R. J.; Eggers, D. F.; Wiberg, K. B. *J. Chem. Phys.* **1959**, *30*, 512.
(19) Wiberg, K. B. *Angew. Chem.* **1986**, *98*, 312.

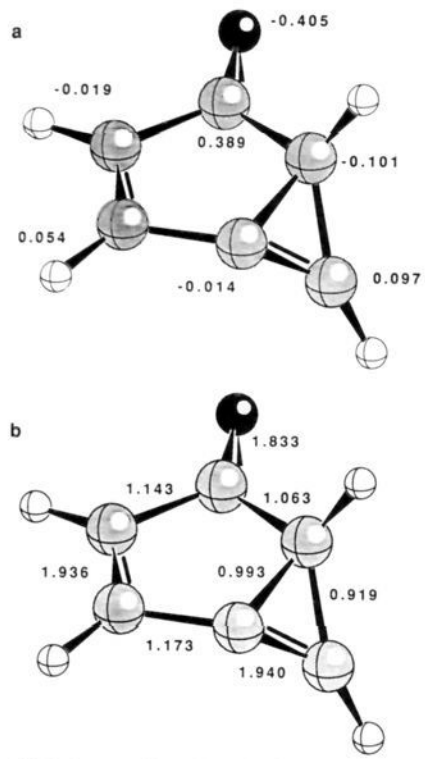

Figure 6. RMP2 charges (a) and bond orders (b) of compound **4**. CH group charges are given for C1, C3, C4, and C6.

is very high, and therefore it can be concluded that despite the distortion of the double bond C5–C6 the ground state of **4** is singlet.

Inspection of Figure 5 reveals that despite the unfavorable folding angle between three- and five-membered ring (129.6°) a strong distortion of the C5–C6 double bond is avoided by the molecule. Thus, the torsional angle between the two carbon 2pπ-orbitals is just 9°, and the pyramidalization angles at C5 and C6 are just 19.2 and 5.5°, respectively.[20] Test calculations for ethylene using these distortion angles and the C5–C6 bond length of 1.317 Å reveal that the RMP2/6-31G(d) energy increases only moderately by 9.1 kcal/mol upon distorting the ethylene double bond to the geometry it possesses in **4**. Similar observations have also been made by other researchers.[21]

Figure 6 displays MP2/6-31G(d) atomic charges and bond orders, where the latter have been evaluated from the MP2 response density at the bond critical points.[22,23] The bond orders reveal that the formal single bonds C1–C2, C2–C3, and C4–C5 all possess partial double bond character typical of π-conjugation in nonaromatic polyenes or cyclopolyenes.[22b]

It is interesting to note that π-conjugation in the five-membered ring is stronger than a peripheral π-conjugation including the cyclopropene ring. Hence, the electronic structure of **4** is closer to form a than form b.

(20) In Figure 5, it is assumed that the 2pπ-orbital at C5 (C6) forms the same angle α with the three bonds C5–C1, C5–C4, and C5–C6 (C6–C1, C6–C5, and C6–H). The pyramidalization angle is defined as $\alpha - 90°$.

(21) Jemmis, E. D.; Schleyer, P. v. R. *J. Am. Chem. Soc.* **1982**, *104*, 4781.

(22) (a) Cremer, D.; Kraka, E. *Croat. Chem. Acta* **1984**, *57*, 1259. (b) Kraka, E.; Cremer, D. The Concept of the Chemical Bond. *Theoretical Models of Chemical Bonding*; Springer: Berlin, 1990; Part 2, p 453.

(23) The bond order n is given by the equation $n = \exp[a(\rho_b - b)]$ (ref 22), where ρ_b is the electron density at the bond critical point and the two constants a and b have been determined from ρ_b(ethane) and ρ_b(ethene) at MP2/6-31G(d)//MP2/6-31G(d) to be 1.075 and 1.657, respectively.

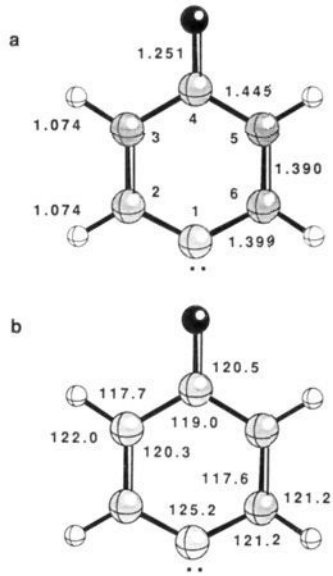

Figure 7. UHF/6-31G(d) structure of **5**: (a) bond lengths, (b) bond angles.

In Figure 6a, the calculated MP2/6-31G(d) charges are given. They indicate that the electrophilic centers are C2, C6, and C4 while the nucleophilic centers are C1, C3, and C5. The calculated MP2 dipole moment is 3.2 D (approximate direction from C5–C6 bond (positive end) toward O (negative end)), which is comparable to the dipole moment found for cyclopentanone (3.3 D).[24]

Strain Energy and Heats of Formation of 4. The homodesmotic strain energy of cyclopropene, c-C_3H_4, defined by the formal reaction eq 1, is known to be 53 kcal/mol.[19,25] Comparison of

$$\text{c-}C_3H_4 + CH_2{=}CH_2 + 2CH_3CH_3 \rightarrow CH_3CH_2CH_3 + 2CH_2{=}CHCH_3 \quad (1)$$

the strain energy of **4** with that of cyclopropene with the aid of formal reaction eq 2 reveals that **4** possesses within 1 kcal/mol (MP2/6-31G(d) reaction energy 0.1 kcal/mol) the same strain energy as cyclopropene. This result is confirmed when the

$$\mathbf{4} + CH_2{=}CH_2 + 5CH_3CH_3 \rightarrow \text{c-}C_3H_4 + 2CH_3CH_2CH_3 + 2CH_2{=}CHCH_3 + (CH_3)_2C{=}O \quad (2)$$

homodesmotic strain energy of **4** is explicitly calculated with the formal reaction eq 3 and the difference of reaction energies (eqs 1 and 3) is taken. This is 1.4 kcal/mol in agreement with the

$$\mathbf{4} + CH_2{=}CH_2 + 5CH_3CH_3 \rightarrow (CH_3)_3CH + 3CH_2{=}CHCH_3 + CH_2{=}C(CH_3)_2 + (CH_3)_2C{=}O \quad (3)$$

result obtained for reaction eq 2. Hence, the homodesmotic strain energy of **4** is 54 ± 1 kcal/mol. With use of this value and known heats of formation for the compounds in reaction eq 3,[26] $\Delta H_f°$ of **4** is estimated to be 57 kcal/mol.

The calculated result that **4** and cyclopropene possess the same strain energy is astonishing in view of the extra strain introduced by distorting the cyclopropene double bond in the bicyclus. This strain energy can be assessed by considering the formal reaction eq 4, where cyclopentadienone rather than cyclopent-2-enone is

$$\mathbf{4} + CH_2{=}CH_2 \rightarrow \text{c-}C_3H_4 + \text{cyclopentadienone} \quad (4)$$

used as a reference compound because of calculational reasons. The MP2/6-31G(d) energy of reaction eq 4 is −14.5 kcal/mol,

(24) Lide, D. R.; Maryott, A. A. *NSRDS-NBS* **1967**, *10*.

(25) George, P.; Trachtman, M.; Block, C. W.; Brett, A. M. *Tetrahedron* **1976**, *32*, 1357.

(26) Cox, J. D.; Pilcher, G. *Thermochemistry of Organic and Organometallic Compounds*; Academic Press: New York, 1970.

which provides upper bound to the extra strain since the bond C1–C5 in **4** is not a double bond. This estimate of the extra strain energy has to be compared with the energy increase 9.1 kcal/mol (vide infra) calculated upon distorting ethylene to the geometry it adopts in the cyclopropene part of **4**. We conclude that the extra strain energy is between 9 and 14 kcal/mol.

The stabilization energy of a hexatriene by π-conjugation is about 20 kcal/mol.[25] Of course, π-conjugation in **4** is weakened by distortion of the double bond in the three-membered ring, and therefore the π-stabilization energy of **4** will be between that of *trans*-butadiene (7 kcal/mol[25]) and hexatriene. This is sufficient to compensate for the extra strain caused by the bicyclic structure of **4**. The calculated total strain energy of **4** reveals that extra strain and π-conjugation energy cancel each other out, thus leading to a strain energy of **4** identical with that of cyclopropene.

Infrared Spectrum of 4. Convincing proof that A is identical with **4** is given by a comparison of experimental and calculated RHF/6-31G(d) IR spectrum (Figure 3 and Table IV). In the range between 3100 and 500 cm^{-1}, all observed fundamental vibrations (ν_6–ν_{27}) have been reproduced within several wave numbers. The relative intensities, deuterium, and ^{18}O shifts are also in good agreement and have been used to assign experimental and calculated vibrations. A weak band at 1165.8 cm^{-1}, which has no counterpart in the calculated spectrum, is assigned to an overtone to the strong fundamental ν_6 at 583.4 cm^{-1} (Figure 3, Table IV). Due to their weakness and overlap between reactant and product peaks, there are some uncertainties in the assignment of the C–H stretching modes ν_{24}–ν_{27} around 3000 cm^{-1}. The largest deviation between experiment and calculation is found for the C=O stretching mode (ν_{23}), the calculated (scaled) frequency being too high by 65 cm^{-1}. The C=O bond length is calculated at RHF/6-31G(d) to be 1.187 Å, which is shorter than both the RHF/3-21G and the MP2/6-31G(d) values. The RHF/3-21G calculated frequency is closer to the experimental value, but the correspondence of other vibrations and especially of the band intensities is rather poor. MP2/6-31G(d) calculations of frequencies have not been possible due to the size of the molecule.

The enone system of **4** is characterized by the carbonyl absorption (ν_{23}, 1713.4 cm^{-1}) and a weak absorption at 1520.6 cm^{-1} assigned to the C=C stretching vibration of the five-membered ring (ν_{21}). This assignment is confirmed by the observed (in parentheses calculated) isotopic shifts: In [d_4]**4**, ν_{23} is shifted by −6.7 (−2.7) cm^{-1} and ν_{21} by −45.3 (−48.5) cm^{-1}, while in [^{18}O]**4** ν_{23} is shifted by −24.1 (−33.5) cm^{-1} and ν_{21} by −1.1 (−0.5) cm^{-1} (Table IV). The corresponding vibrations in model compound **14a** are located at 1698.5 (vs) and 1571.7 (w) cm^{-1}.

A medium-intensity band at 1665.2 cm^{-1} showing a deuterium shift of −41.9 cm^{-1} and an ^{18}O shift of −3.8 cm^{-1} (calculated −54.8 and −2.1 cm^{-1}, respectively) is assigned to the C=C stretching vibration ν_{22} of the three-membered ring (Table IV). Cyclopropenes with similar patterns of substitution exhibit deuterium shifts around −40 cm^{-1} but absorb above 1740 cm^{-1}. For two derivatives of bicyclo[4.1.0]heptatriene, Chapman et al. reported C=C stretching vibrations at 1755 and 1765 cm^{-1}, respectively.[27] Obviously the higher distortion of the C5–C6 bond in **4** leads to an absorption at lower frequencies.

A weak band at 1680.2 cm^{-1}, which is not a fundamental vibration according to the calculations, is assigned to a Fermi resonance between ν_{23} (1713.4 cm^{-1}) and an overtone of ν_{11} (2 × ν_{11} 1686.4 cm^{-1}). ^{18}O substitution shifts ν_{23} to lower frequencies (1689.3 cm^{-1}) but hardly effects ν_{11} (2 × ν_{11} 1683.6 cm^{-1}), and thus both vibrations are now in close proximity. Fermi resonance leads to a decrease of the intensity of ν_{23} and to a tremendous increase in the intensity of 2 × ν_{11}, which becomes close to the intensity of the carbonyl absorption.

UV–Vis Spectrum of 4. The striking similarity of the UV–vis spectra of **4** and **14a** (Figure 1 and Table V) is due to the cyclopentenone chromophore in both molecules. The major difference in the spectrum of **4** compared to that of **14a** is a broad band of medium intensity with λ_{max} at 418 nm and extension to 500 nm, which is associated with the highly strained cyclopropene ring. Irradiation into the long wavelength part of this band causes the rapid isomerization to carbene **5**. The UV–vis spectrum of **4** can be reproduced by CNDOS calculations (Table V). The longest wavelength transition calculated at 432 nm is described best as the $\pi \rightarrow \pi^*$ transition of the cyclopropene moiety. The transition moment is directed approximately perpendicular to the C=O bond in the plane of the enone system.

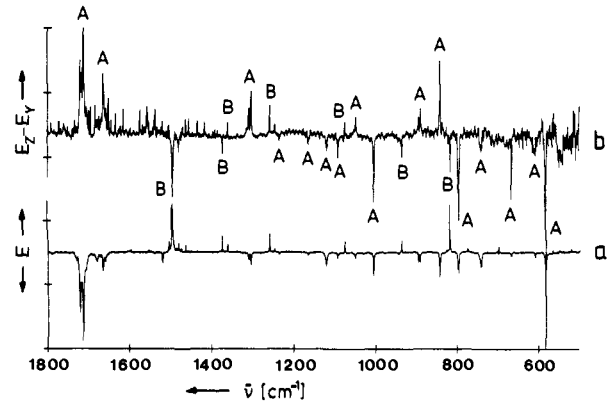

Figure 8. IR spectra of the photochemistry **4** → **5**: (a) difference spectrum, bottom part showing bands disappearing (assigned to **4**) and top part showing bands appearing on irradiation (λ = 436 nm), (b) polarized difference spectrum, bottom part showing bands polarized perpendicular to **E** and top part showing bands polarized parallel to **E**. (A) bands assigned to **4**. (B) bands assigned to **5**.

Photoselection of 4 and 5

Photoselection has been shown by Turner et al.[10] and by Thulstrup and Michl[28] to be useful in producing partially oriented samples of matrix-isolated species. We used this method to obtain information about the symmetry of **4** and **5**. The principle of photoselection is to correlate the laboratory coordinate system with the internal coordinate system of molecules trapped in rigid media to prevent molecular rotation. The laboratory coordinate system is defined by the direction of the propagation of light (X) and by the direction of the electric field vector **E** (Z). In carbene **5** with C_{2v} symmetry, the internal coordinate system is defined by the direction of the C–O bond (z), the plane that contains the atoms (yz-plane), and the direction perpendicular to this plane (x). In analogy, we define the internal coordinate system of the unsymmetrical bicyclus **4** by the direction of the C–O bond (z), the plane that contains the enone system (yz-plane), and the direction perpendicular to this plane (x).

When **4**, matrix-isolated in argon at 10 K, was irradiated (λ = 436 nm) with linearly polarized light to 30–60% conversion, remaining **4** as well as newly formed **5** exhibited pronounced IR dichroism (Figure 8, Tables I and IV). In a typical experiment, the dichroic ratios $d_\nu = \mathbf{E}_Z/\mathbf{E}_Y$ of vibrations in **4** vary between 0.55 and 1.54 and in **5** between 0.85 and 1.19, which indicates, in accordance with theory,[28] a higher degree of orientation for the remaining **4** as for the newly formed **5**. The dichroic ratios d_ν have been obtained by integrating peak intensities or by measuring peak heights. Errors of d_ν are estimated to be 3% for intense peaks and in excess of 5% for weak peaks. Because of the low symmetry of **4** and the lack of experimental data about the direction of the transition moment of the visible band responsible for the observed photochemistry, the results from photoselection experiments are interpreted in qualitative manner only.

The transition moment of the C–O vibration of **4** with d_{1713} = 1.16 ± 0.03 is aligned parallel to Z, while that of the C–O vibration of **5** with d_{1496} = 0.89 ± 0.04 is aligned perpendicular to Z. The interpretation of the results for **5** is straightforward:

(27) West, P. R.; Mooring, A. M.; McMahon, R. J.; Chapman, O. L. *J. Org. Chem.* **1986**, *51*, 1316.

(28) Thulstrup, E. W.; Michl, J. *Elementary Polarization Spectroscopy*; VCH: New York, 1989.

Only two classes of dichroic ratios are observed, $d_y = 0.89 \pm 0.04$ and $d_y = 1.17 \pm 0.04$, which means that **5** is of C_{2v} symmetry. The out-of-plane deformation mode at 819 cm^{-1}, which is x-polarized, shows $d_{819} = 0.93 \pm 0.04$ and thus belongs to the same class as the z-polarized C–O stretching mode. Thus, x and z are indistinguishable, and the molecule is aligned along its y direction. Vibrations with positive d_y are polarized in the y direction; vibrations with negative d_y are polarized in the x or z direction. This alignment corresponds to a transition moment of the visible absorption mainly in the y direction as it is predicted by the CNDOS calculation.

Bicyclus **4** shows a variety of different dichroic ratios as is expected for an unsymmetrical molecule. This additional information was used to assign bands of **4** and [d_4]**4**. The largest dichroic ratio is observed for ν_{22} ($d_{1665} = 1.54$, Table IV), which means that the direction of polarization of this band is closest to the direction of the visible transition moment. If one assumes that ν_{22} is polarized approximately along the C5–C6 bond, the visible absorption must be polarized close to that direction, which is in qualitative agreement with the CNDOS calculations. For a pure $\pi \rightarrow \pi^*$ transition of the cyclopropene system, the expected polarization would be the direction of the C5–C6 bond. Due to the large uncertainties in the location of the visible transition moment direction, angles between this transition and IR transitions have not been determined.

Kinetics

Reaction rates of the **4** → **5** rearrangement have been measured in argon, xenon, and nitrogen matrices, the [d_4]**4** → [d_4]**5** rearrangement in argon and xenon matrices. Additionally, some experiments have been carried out in krypton. IR-induced rearrangements (using a Ge filter to block visible light from the globar as IR source) as well as thermal rearrangements (using long pass IR filters to cut off short-wavelength IR radiation) have been investigated. Some care has been taken to discriminate thermal and IR-induced rearrangements. With a long pass filter with 50% transmission at 1880 cm^{-1}, the same kinetics was observed no matter whether the matrix was irradiated all the time or the beam was blanked off between the measurements. In the latter case, the matrix was exposed to IR irradiation at 5% of the total time only. Therefore, this filter was used to obtain reliable kinetic data for the thermal rearrangement. Additionally, the IR beam was blanked off between measurements.

Evaluation of Kinetic Data. For IR-induced rearrangements, analysis according to first-order kinetics gave excellent fits of experimental data. In this case, molecules in different matrix sites do not differ much in their kinetic behavior. More quantitative information about the distribution of matrix sites comes from an empirical formula described by Siebrand and Wildman:[29]

$$A \rightarrow B \tag{5}$$

$$[A]_t = [A]_0 \exp[-(k_1 t)^{\beta}] \tag{6}$$

For an exponential rate process, β is 1; in glassy matrices with multiple sites, typical values are close to 0.5.[29] In our hands, fitting of eq 6 to the data for IR-induced rearrangements gave $\beta = 0.9$–1, which means that there is a narrow distribution of matrix sites differing in their kinetic behavior. For thermal rearrangements, the rates depend more on the matrix surrounding and lower values (0.6–0.8) have been calculated for β. This difference in the thermal and IR-induced rearrangement can be rationalized if one considers the different amount of energy available for the rearranging molecules. The thermal energy available at low temperatures is very small, and small differences in the energies of activation caused by different matrix sites translate to substantial differences in reaction rates. On the other hand, the amount of energy available from IR irradiation (see below) is high and the rates depend mainly on the photon flux.

IR-Induced Rearrangement. When the matrix (argon at 10 K) was irradiated continuously by using a long pass filter with 50% transmission at 5000 cm^{-1}, the rates for the rearrangement **4** → **5** were 50–60 times higher than without IR irradiation. In other matrices (xenon, krypton, and nitrogen), similar results were observed. A long pass filter with 50% transmission at 2700 cm^{-1} caused only doubling of the rates, which indicates that 5000–2700 cm^{-1} irradiation is much more effective than irradiation at lower wave numbers. This filter (50% transmission at 2700 cm^{-1}) has a transmission of 85% in the C–D stretching region (2247–2294 cm^{-1}) but no transmission in the C–H stretching region (3008–3085 cm^{-1}). From that, we conclude that not excitation of C–D stretching modes—and probably not of C–H stretching modes—increases the rates, but rather irradiation into some high-frequency overtone.

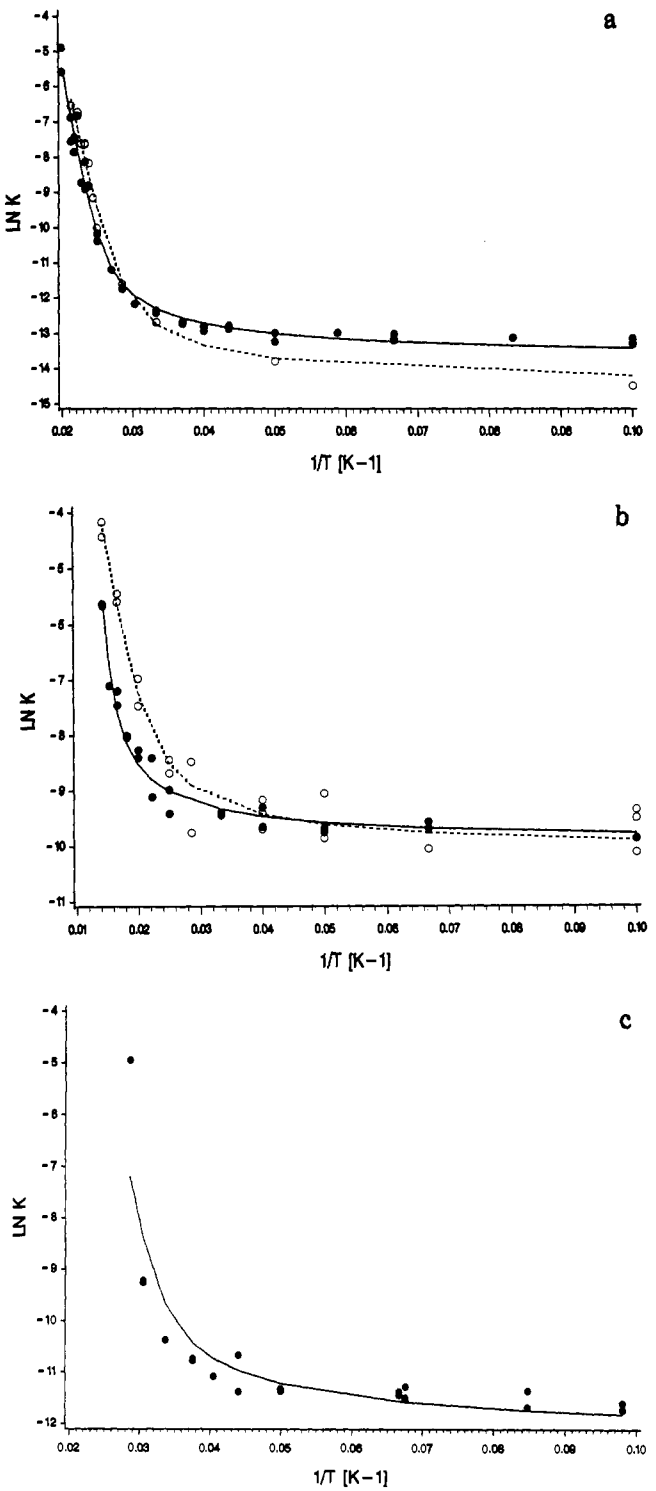

Figure 9. Arrhenius plots for the rearrangements **4** → **5** (solid dots and curve) and [d_4]**4** → [d_4]**5** (open dots and dashed curve): (a) argon matrix, (b) xenon matrix, (c) nitrogen matrix.

(29) Siebrand, W.; Wildman, T. A. *Acc. Chem. Res.* **1986**, *19*, 238.

Thermal Rearrangement. Arrhenius plots have been obtained for the thermal rearrangement of **4** in argon, xenon, and nitrogen matrices and for [d_4]**4** in argon and xenon matrices (Figure 9a–c). In all cases, a nonlinear Arrhenius behavior is observed. Below approximately 25 K (exact temperature depending on the matrix), the reaction rates are independent of temperature in all matrices. This unusual temperature dependence indicates that tunneling is important at low temperature. Similar Arrhenius plots have been described by Buchwalter and Closs for the cyclization of 1,3-cyclopentanediyl,[30] by Dougherty et al. for the cyclization of 1,3-cyclobutanediyl,[31] and for several cases of spin-forbidden proton tunneling.[32a,b] Heavy atom tunneling has also been proposed for the interconversion of the cyclobutadiene valence tautomers.[32c,33b] At higher temperature, classical behavior is observed. The shape of the Arrhenius plots depends on the matrix used and additionally shows some differences between **4** and [d_4]**4**.

Several points have to be taken into account for the interpretation of the Arrhenius plots:

Mechanical properties of matrices strongly depend on temperature. The observed curvature of Arrhenius plots might reflect properties of matrices rather than properties of matrix-isolated molecules. At temperatures above 30% of their melting point (mp: N_2, 63.2 K; Ar, 83.3 K; Xe, 161.4 K), matrices become less rigid and thus intramolecular rearrangements might become faster. The interpretation of the experimental data solely on matrix effects requires that the rearrangement has no classical barrier in the gas phase. The observed temperature dependence is then caused by the matrix cage, which resists changes in the shape of isolated molecules. From this, it follows that the matrix only effects the Arrhenius preexponential factor A (eq 7) and thus the entropy of activation and not the height of the barrier E_a. There is no indication for this type of interaction nor for the absence of a thermal barrier in the gas phase. More reasonable is that both intrinsic properties of the isolated molecules and matrix effects determine the shape of the Arrhenius plots.

At temperatures above 50% of the melting point of matrices, diffusion of trapped species becomes important. Thus, at these temperatures, intermolecular rather than intramolecular reactions might be dominant. Dimerization of carbene **5** is expected to proceed with only a small barrier or even without barrier of activation, and therefore the rate of the thermal disappearance of **5** reflects the mobility of **5** in the matrix. In argon above 40 K, **5** disappears rapidly, while below that temperature the carbene is stable for many hours. Below 35 K, no change is observed even after several days. It was not possible to obtain values for the barrier of activation of the dimerization of **4**, but if this barrier is low, in the high temperature range dimerization can compete with rearrangement. As expected, below 35 K in Ar matrices, the kinetics of the disappearance of **4** matches the kinetics of the appearance of **5** and dimerization is not important. At higher temperatures, the disappearance of **4** is faster than the appearance of **5**. This means that dimerization of **4** or **5** or both becomes significant, and thus a systematic error might appear in the high-temperature part of the Arrhenius plots. Because of the low melting point of nitrogen, dimerization becomes significant above 30 K and thus kinetic data for the rearrangement in nitrogen are less reliable. On the other hand, in xenon even at 70 K, dimerization is not observed. Xenon matrices allow one to obtain kinetic data in the widest temperature range.

Two approaches have been used for the evaluation of the Arrhenius plots. One approach is to look at the plots as superposition of two linear plots, one describing the classical behavior at high temperature and one describing the tunneling part at low temperature (Figure 9). The other approach is to use a modified Arrhenius equation (eq 8) developed by Bell[33a] by using a parabolic barrier as a model.

Scheme III

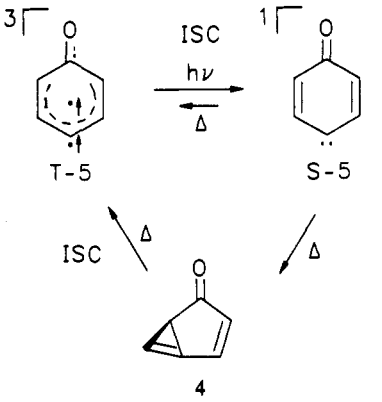

Table VII. Reaction Rates[a] k_T for the Rearrangement of **4** and [d4]**4** in Argon, Krypton, Xenon, and Nitrogen Matrices ($k \times 10^7$ s^{-1})

T (K)	Ar, **4**	Ar, [d_4]**4**	Kr, **4**	Xe, **4**	Xe, [d_4]**4**	N_2, **4**
10	14	5	69	520	400	54
20	14	10		630	530	97
30	13	31		830	1300	230
40	350	450		1300	1700	
50	33 000			2500	6500	
60				5800	43 000	
70				37 000	160 000	

[a] The disappearance of **4** has been used to calculate the rates. In Xe, this is in good accordance with the appearance of carbene **5**; in Ar above 35 K and in N_2 above 30 K, **4** disappears more rapidly than **5** is formed due to intermolecular processes.

$$k = A \exp(-E_a/RT) \quad (7)$$

$$k = QA \exp(-E_a/RT) \quad (8)$$

$$Q = (e^{\alpha}/\beta - \alpha)(\beta e^{-\alpha} - \alpha e^{-\beta})$$

$$\alpha = E_a/RT \qquad \beta = 2\pi^2 d(2mE_a)^{1/2}/h$$

Equation 8 has been used by Buchwalter and Closs[30] as well as by Dougherty et al.[31] to calculate E_a and the tunneling distance d for a given mass of the tunneling particle m. As it has been pointed out by Dougherty, only the product $dm^{1/2}$ can be optimized effectively and the choice of m (or d) is arbitrary.[31] The curves in Figure 9 and the activation parameters in Table VIII have been obtained by using $m = 12$ and fitting the other parameters in eq 8 with the experimental data. A similar fit could be obtained if $m = 92$, the mass of the molecule, was used. With this value, only the calculated tunneling distance is reduced (Table VIII).

Activation Parameters. The Arrhenius parameters have been used to calculate the activation enthalpy $\Delta H^{\ddagger}$ and entropy $\Delta S^{\ddagger}$ according to eqs 9 and 10 (Table VIII). Because of the limited temperature range of the measurements, the error of the data in

$$\Delta H^{\ddagger} \approx E_a - RT \quad (9)$$

$$\Delta S^{\ddagger} = R \ln [k(h/k_{\beta}T) \exp(-\Delta H^{\ddagger}/RT)] \quad (10)$$

$$k = A \exp(-E_a/RT)$$

Table VIII is quite large, especially for nitrogen and argon matrices. For nitrogen matrices, it is not possible to obtain activation parameters for the classical part of the Arrhenius plots. Nevertheless, some important information can be extracted from the kinetic data.

Independent of the method of evaluation and the matrix material used, E_a for the **4** → **5** rearrangement is calculated between 2.0 and 2.7 kcal/mol. The lower value is obtained in N_2 and is subject to a larger error as it was mentioned above. Thus, the most reasonable value for E_a is 2.6 ± 0.2 kcal/mol.

The Arrhenius factor A is very low, and the corresponding

(30) Buchwalter, S. L.; Closs, G. L. *J. Am. Chem. Soc.* **1979**, *101*, 4688.
(31) Sponsler, M. B.; Jain, R.; Coms, F. D.; Dougherty, D. A. *J. Am. Chem. Soc.* **1989**, *111*, 2240.
(32) (a) McMahon, R. J.; Chapman, O. L. *J. Am. Chem. Soc.* **1987**, *109*, 683. (b) Fisher, J. J.; Michl, J. *J. Am. Chem. Soc.* **1987**, *109*, 583. (c) Orendt, A. M.; Arnold, B. R.; Radziszewski, J. G.; Facelli, J. C.; Malsch, K. D.; Strub, H.; Grant, D. M.; Michl, J. *J. Am. Chem. Soc.* **1988**, *110*, 2648.
(33) (a) Bell, R. P. *The Tunnel Effect in Chemistry*; Chapman and Hall: London, 1980. (b) Carpenter, B. K. *J. Am. Chem. Soc.* **1983**, *105*, 1700.

Table VIII. Activation Parameters for the Rearrangement of **4** and [d_4]**4** in Argon, Xenon, and Nitrogen Matrices

	Ar, **4**	Ar, [d_4]**4**	Xe, **4**	Xe, [d_4]**4**	N_2, **4**
			Arrhenius, Classical Part[a]		
E_a (kcal/mol)	2.1 ± 0.3	1.7 ± 0.2	2.6 ± 0.7	1.0 ± 0.5	
$\Delta H^{\ddagger}$ (kcal/mol)	2.0 ± 0.3	1.6 ± 0.2	2.5 ± 0.7	0.9 ± 0.5	
log A	6.1 ± 1.5	4.0 ± 1.1	4.9 ± 1.1	1.1 ± 0.6	
$\Delta S^{\ddagger}$ (cal/K)	−22 ± 12	−29 ± 12	−29 ± 12	−50 ± 12	
			Arrhenius, Tunnel Part[b]		
E_a (cal/mol)	6.0 ± 2.9	ca. 0	9.6 ± 2.4	2.9 ± 1	11.2 ± 4.1
$\Delta H^{\ddagger}$ (cal/mol)[c]	0	0	0	0	0
log A	−4.7 ± 1.5	−5.3 ± 1	−3.4 ± 1	−3.5 ± 1	−4.0 ± 1.5
$\Delta S^{\ddagger}$ (cal/K)	−79 ± 7	−81 ± 7	−72 ± 7	−72 ± 7	−77 ± 7
			Bell[d]		
E_a (kcal/mol)	2.6 ± 0.2	2.1 ± 0.1	2.8 ± 0.4	1.6 ± 0.2	2.0 ± 0.1
$\Delta H^{\ddagger}$ (kcal/mol)	2.5 ± 0.2	2.0 ± 0.1	2.6 ± 0.4	1.5 ± 0.2	1.9 ± 0.1
log A	7.0 ± 0.1	5.4 ± 0.3	4.3 ± 1.1	2.2 ± 0.6	7.2 ± 0.6
$\Delta S^{\ddagger}$ (cal/K)	−17 ± 12	−26 ± 12	−34 ± 14	−43 ± 12	−16 ± 10
d (Å)[e]	0.41 ± 0.02	0.41 ± 0.04	0.27 ± 0.02	0.26 ± 0.01	0.45 ± 0.04

[a] Equation 7, for the calculation of the enthalpy of activation $\Delta H^{\ddagger}$ (eq 9) and entropy of activation $\Delta S^{\ddagger}$ (eq 10), T is set to 45, 60, and 33 K in Ar, Xe, and N_2, respectively. [b] Equation 3, for the calculation of $\Delta H^{\ddagger}$ and $\Delta S^{\ddagger}$, T is set to 10 K in all matrices. [c] Set to 0. [d] Equation 8, for the calculation of $\Delta H^{\ddagger}$ and $\Delta S^{\ddagger}$, T is set to 45, 60, and 33 K in Ar, Xe, and N_2, respectively. [e] Tunneling distance.

entropies of activation $\Delta S^{\ddagger}$ are highly negative as is expected for a spin-forbidden reaction. In argon and nitrogen, evaluation according to Bell (eq 8) gives log A = 7, which is in the order of values typical for reactions that require spin inversion.[30-32a,b] From that, we conclude that the rate-determining step is the intersystem crossing (ISC) and **4** is directly transformed into T-**5** without S-**5** as an intermediate (Scheme III).

In the Arrhenius plots (Figure 9), some matrix effects are easily recognized. In argon and nitrogen, the curves start to rise at lower temperatures than in xenon, which is explained by increasing rates of dimerization of **4** at temperatures above 50% of the melting point of the matrix. Thus, activation parameters calculated from the Arrhenius plots are more reliable in Xe than in Ar or N_2. In xenon, the rearrangement is generally faster than in argon or nitrogen (Table VII). Only at 50 K, intermolecular processes in argon cause a larger value of k_{50} (rate of the disappearance of **4** at 50 K) than in xenon. At 10 K, where the only contribution to the rates comes from tunneling, the relative rates k_{10} in Ar, N_2, Kr, and Xe are 1:4:5:37.

Evaluation of the data according to Bell's formula (eq 4) reveals that the faster reaction in xenon compared to that in other matrices is not reflected by a lower energy of activation $\Delta H^{\ddagger}$ or a less negative entropy of activation $\Delta S^{\ddagger}$ but rather by a smaller tunneling distance d (0.27 Å in Xe, 0.41 Å in Ar, and 0.45 Å in N_2). The calculated d is independent of deuteration (Table VIII). Setting into eq 4 other fixed values for d gives only poor fits of the experimental data. It is obvious that d reflects not only molecular properties of **4** and **5** but also some matrix properties. As mentioned above, the values obtained in argon and nitrogen are considered less reliable than those in xenon.

A significant kinetic deuterium isotope effect k_H/k_D is observed, but again the matrix environment plays an important role. In xenon, the tunneling rates for **4** and [d_4]**4** are similar (at 10 K, k_H/k_D = 1.3, Table VII), while in the classical part of the Arrhenius plot (Figure 9b) an inverse kinetic deuterium effect is observed (at 50 K, k_H/k_D = 0.38). In argon, the kinetic isotope effect in the tunneling region is more pronounced (at 10 K, k_H/k_D = 2.75) but by far too small for proton tunneling.[32b,33a] At higher temperatures again, an inverse kinetic deuterium effect is observed, although much smaller than in xenon (at 40 K, k_H/k_D = 0.78, Table VII). Independent of the method of evaluation, E_a is smaller for the deuterated compounds, the most reasonable value being 1.7 ± 0.2 kcal/mol (Table VIII). Despite the complications caused by matrix effects, it is clear that the deuterium effect is small and hydrogen shift can be ruled out in the rate-determining step. Thus, the observed tunneling must be heavy atom tunneling.

Obviously matrix effects and kinetic isotope effects can not be discussed independently of each other. A possible explanation for the higher rates in xenon compared to those in other matrices is the external heavy atom effect induced by Xe atoms and to a lesser extent by Kr atoms. From the higher rates k_{10} in N_2 compared to those in Ar (Table VII), it is clear that this cannot be the only explanation and that there must be other properties of the matrix influencing the ISC. Inverse kinetic deuterium isotope effects have been described by Jortner et al.[34] for the S_1–T_1 ISC of anthracene and by Eisenthal et al.[35] for the ISC of diphenylmethylene. A prerequisite for this phenomenon is a small energy gap ΔE_{ST} (<2500 cm^{-1}), which means that there is a low density of final states in the triplet manifold available from the singlet state. Deuteration leads to a higher density of triplet states and thus to a better off-resonance coupling between the singlet state and triplet vibronic levels.[34,35] The small energy gap ΔE_{ST} does not only lead to the inverse isotope effect but also to an inverse solvent energy gap effect. Solvents decreasing ΔE_{ST} also decrease the rate of the intersystem crossing k_{ST}.[35]

The effect of solvation on ΔE_{ST} is to stabilize or destabilize the singlet or triplet state depending on their relative polarities and on the solvent polarity. As can be seen from Table V, in xenon the longest wavelength absorption of **4** is blue-shifted by 1200 cm^{-1} compared to that in argon; in nitrogen, a red shift of 150 cm^{-1} is found. A similar solvent effect is not observed for carbene T-**5**. Xenon has a higher polarizability than argon, and thus the polar ground state of **4** (calculated 3.2 D) is better stabilized in xenon, while the less polar excited state is less effected by the solvent. We conclude that **4** is more polar than T-**5**, which is in accordance to our ab initio calculations. From that follows that, in xenon, the energy gap between **4** and **5** is reduced compared to argon. If the assumption of a small singlet–triplet energy gap holds for this system, we expect in the order xenon, krypton, argon, and nitrogen, with decreasing polarizability, an increase of k_{ST} and a decrease of the inverse kinetic deuterium effect. The external heavy atom effect, which influences only k_{ST}, shows just the opposite order, with xenon being most efficient. The observed order for the rates of the **4** → **5** rearrangement can be rationalized if in krypton and xenon the heavy atom effect dominates while in nitrogen and argon the polarizability is more important and thus in argon the lowest rates at a given temperature are observed (Table VII). The inverse kinetic deuterium effect depends only on the energy gap and thus is larger in xenon than in argon.

Conclusion

Triplet carbene **5** and bicyclus **4** can be produced in a photostationary equilibrium. Irradiation into the longest wavelength triplet–triplet absorption band of T-**5** produces high yields of **4**; irradiation into the $\pi \rightarrow \pi^*$ transition of **4** yields **5** in a completely reversible manner. The most reasonable route from T-**5** via its

(34) Amirav, A.; Sonnenschein, M.; Jortner, J. *Chem. Phys. Lett.* **1983**, *100*, 488.

(35) Langan, J. G.; Sitzmann, E. V.; Eisenthal, K. B. *Chem. Phys. Lett.* **1986**, *124*, 59.

excited state T-5* includes S-5 as an intermediate. In this case, the thermal rearrangement of S-5 to 4 must be fast compared to the intersystem crossing (ISC) back to T-5 and the heat of formation of 4 (calculated to 56.9 kcal/mol, vide infra) higher than that of T-5 but lower than that of S-5 (Scheme III).

An alternative route for the observed photochemistry, which does not require singlet carbene S-5 as an intermediate, is the formation of 4 in its T_1 state (T-4) from T-5* and subsequent ISC to S-4. This requires that T-4 can be populated thermally from T-5*. The energy of T-4 is quite high (ca. 104 kcal/mol above S-4, vide infra), while T*-5 lies only 50.7 kcal/mol above T-5 (Table II). If the energy gap between T-5 and S-4 is small—as we assume—T*-5 lies below T-4, and therefore this route can be ruled out.

From our kinetic studies, the following conclusions can be drawn for the thermal rearrangement S-4 → T-5:

(1) The rearrangement must be exothermic, and thus S-4 is higher in energy than T-5. The absolute energy difference is not known, but if the assumption of a small energy gap holds, it cannot be larger than 2500 cm^{-1}.

(2) Very low Arrhenius factors A are observed as is expected for a "spin-forbidden" process. The ISC is the rate-determining step.

(3) The activation barrier E_a is 2.6 ± 0.2 kcal/mol and on deuteration is reduced to 1.7 ± 0.2 kcal/mol.

(4) At low temperatures, heavy atom tunneling is observed. The calculated tunneling distance of 0.3 Å is in accordance with geometric changes necessary to transform 4 to 5.

Bicyclus 4 is a compound of fleeting existence even under the conditions of matrix isolation at 10 K. Ab initio calculations reveal that the strain energy of 4 is 54 ± 1 kcal/mol, comparable to the strain energy of cyclopropene.

The thermal rearrangement S-4 → T-5 requires both geometric changes and ISC and is, thus, both spin and Franck–Condon forbidden. Our data require that ISC be rate determining and T-5 be formed directly without formation of S-5 as an intermediate. If S-5 was an intermediate and the ISC S-5 → T-5 rate determining, the singlet carbene should build up in detectable quantities.

Experimental Section

Materials and General Methods. All reactions were carried out under argon or nitrogen. $H_2{}^{18}O$ (90% isotopic purity) was purchased from Alfa, D_2O (99% isotopic purity) from Aldrich, and 4-aminophenol and $NaBH_4$ from Merck.

4-Diazo-2,5-cyclohexadienone (6). Quinonediazide 6 was synthesized by treating *p*-hydroxybenzenediazonium chloride with silver oxide according to a procedure given by Puza and Doetschmann.[36] The tetrahydrate (yellow needles) was sublimed (45–50 °C, 10^{-5} mbar) to get dehydrated 6 as an orange, microcrystalline material, which explodes when heated above 90 °C: IR (Ar, 10 K) 2076.0 (vs), 1624.7 (vs), 1454.1 (w), 1402.5 (w), 1238.6 (s), 1143.1 (s), 1081.4 (vw), 842.3 (m), 790.7 (w), 770.4 (w), 715.5 (m) cm^{-1}.

[d_4]-4-Diazo-2,5-cyclohexadienone ([d_4]6). [d_7]-*p*-Aminophenol deuteriochloride was synthesized by H–D exchange from *p*-aminophenol hydrochloride according to a general procedure by Werstiuk and Kadai.[37] A 2-g (13.8-mmol) portion of hydrochloride was refluxed in 15 mL of D_2O for 3 h, and then the solvent was evaporated completely. The residue was dissolved in 20 mL of D_2O and heated in a sealed and degassed ampule in an autoclave at 230 °C for 24 h. Evaporation of the solvent gave 2.1 g of [d_7]-*p*-aminophenol deuteriochloride, which was used without further purification. The deuterium content was estimated to be >95% by MS and IR spectroscopy. Quinonediazide [d_4]6 was synthesized as described above: IR (Ar, 10 K) 2079.4 (vs), 1616.5 (s), 1562.1 (s), 1414.1 (w), 1302.2 (m), 1236.1 (w), 1190.3 (vw), 1139.7 (w), 829.7 (w), 812.4 (w), 743.9 (m), 656.2 (m) cm^{-1}.

[^{18}O]-4-Diazo-2,5-cyclohexadienone ([^{18}O]6). In a 3-mL Schlenk tube, 50 mg (0.2 mmol) of 4-nitrobenzenediazonium tetrafluoroborate in 0.3 mL (15 mmol) of $H_2{}^{18}O$ was heated at 90 °C until the evolution of nitrogen had ceased. The excess water was then drawn off by vacuum into another Schlenk tube, which was cooled to 77 K to recover the $H_2{}^{18}O$. The residue was extracted with ether. The whole procedure was repeated five times. The collected ether extracts were purified by column chromatography (SiO_2/Et_2O) and sublimed in high vacuum to give 36 mg (23% of theory) of [1-^{18}O]-4-nitrophenol as a slightly yellow powder.

A solution of 36 mg (0.25 mmol) of the nitrophenol in 1 ml of degassed methanol was slowly added to a suspension of 38 mg (1 mmol) of $NaBH_4$ and 0.25 mg of 10% palladium on carbon in 0.8 ml of degassed H_2O. After stirring at room temperature for 10 min, excess $NaBH_4$ was destroyed by adding sufficient dilute HCl. The catalyst was filtered off, and the solvent was evaporated. The product was extracted from the residue with three 0.5-mL portions of methanol and transformed into the hydrochloride with 0.2 mL of 2 N HCl. Addition of 50 ml of ether gave a precipitate of 27 mg (75%) of [^{18}O]-4-aminophenol hydrochloride as a colorless powder. The quinonediazide [^{18}O]6 was synthesized from the aminophenol as described above, and 3 mg (14% yield) of orange crystals were obtained. The ^{18}O content was estimated by IR spectroscopy to be approximately 75%: IR (Ar, 10 K) 2072.6 (vs), 1605.0 (m), 1358.1 (w), 1238.6 (m), 1143.1 (w), 842.3 (w) cm^{-1}.

Bicyclo[3.1.0]hex-3-en-2-one (14a). Compound **14a** was prepared by a literature procedure:[38] IR (Ar, 10 K): 3142.9 (vw), 3071.8 (w), 3002.6 (w), 1698.5 (vs), 1571.7 (w), 1436.7 (w), 1344.6 (s), 1309.4 (m), 1293.0 (w), 1270.4 (vw), 1228.4 (vw), 1178.8 (m), 1157.6 (w), 1088.6 (w), 1059.2 (w), 1038.5 (w), 988.3 (m), 951.2 (w), 917.5 (m), 856.2 (s), 821.0 (m), 809.5 (m), 766.1 (w), 732.3 (w), 621.0 (w) cm^{-1}.

Matrix Spectroscopy. Matrix isolation experiments were performed by standard techniques with an Air Products CSW-202 Displex closed cycle helium cryostat.[39] Argon (Messer Griesheim, 99.9999%), krypton (Messer Griesheim, 99.99%), xenon (Linde, 99.99%), and nitrogen (Messer Griesheim, 99.9999%) were deposited at 30, 45, 55, and 30 K, respectively, on top of CsI (IR) or sapphire (UV–vis) windows with a rate of approximately 0.15 mmol/min. 4-Diazo-2,5-cyclohexadienone was warmed to 45–48 °C and codeposited. Under these conditions, transparent matrices were obtained after 4 h of deposition time. The temperature range available for kinetic studies was limited by the cryostat to 10 K at the low end and by the vapor pressure of the matrix to 35 (nitrogen), 50 (argon) or 80 K (xenon). To prevent rapid evaporation of N_2 and Ar at temperatures above 30 K, these matrices were capped with xenon.[40]

Infrared spectra were recorded by using a Bruker IFS66 FTIR spectrometer. Standard spectra were taken with a resolution of 1 cm^{-1} in the range 4000–500 cm^{-1}. Polarized IR spectra were recorded by using a Specac polarizer (aluminum grid on TlBr). To avoid visible and IR photolysis of 4, long pass IR filters (Oriel) were used with 50% transmission at 5000 (Ge filter), 2700 (InAs filter), and 1880 cm^{-1} (interference filter on Ge substrate). For IR irradiations, the light source of the FTIR spectrometer in combination with IR filters was used.

Kinetic data have been obtained by integrating the intense carbonyl peaks of 4 and 5. In several experiments, the strong peaks at 819.1 (4) and 583.4 cm^{-1} (5) have been additionally used, giving the same results within error limits. Generally several half-life times have been recorded at higher temperatures. At lower temperatures in Ar, the rearrangement is very slow and spectra have been recorded generally for 20–30 h, in several experiments up to 10 days (taking two spectra per hour) to obtain reliable data.

UV–vis spectra were recorded on a Hewlett-Packard 8452A diode array spectrophotometer with a resolution of 2 nm. An Oriel film polarizer (useful from 300 to 750 nm) was used to obtain linearly polarized light. UV–vis irradiations were carried out with use of Osram HBO 500 W/2 mercury high-pressure arc lamps in an Oriel lamp housing equipped with quartz optics. IR irradiation from the lamps was absorbed by a 10-cm path of water and by a Schott KG1 filter (if only $\lambda > 300$ nm was required). For broad-band irradiation, Schott cut-off filters were used (50% transmission at the wavelength specified); for narrow-band irradiation, interference filters (Schott) in combination with cut-off filters to isolate mercury lines were used. Linearly polarized light was obtained by using a calcite polarizing prism in combination with the filters mentioned above.

Computational Methods. Ab initio calculations have been carried out with restricted and unrestricted Hartree–Fock (RHF and UHF) theory to obtain optimized geometries and vibrational frequencies of compounds 4 and 5. For this purpose, the 3-21G[13a] and 6-31G(d)[13b] basis sets have been employed. RHF/6-31G(d) and UHF/6-31G(d) vibrational frequencies have been scaled by a factor of 0.87.[41]

In order to test the reliability of the RHF geometry of 4, geometry optimization has been repeated with second-order Møller–Plesset per-

(36) Puza, M.; Doetschman, D. *Synthesis* **1971**, 481.
(37) Werstiuk, N. H.; Kadai, T. *Can. J. Chem.* **1974**, *52*, 2169.
(38) Cox, O.; Rivera, L. A. *Synth. Commun.* **1978**, *8*, 261.
(39) Sander, W. W. *Spectrochim. Acta, Part A* **1987**, *43A*, 637.
(40) Swanson, B. J.; Jones, L. H. *J. Mol. Spectrosc.* **1981**, *89*, 566.
(41) Hout, R. F.; Levi, B. A.; Hehre, W. J. *J. Comput. Chem.* **1982**, *3*, 234.

turbation theory (MP2),[14] again by using the 6-31G(d) basis set. The lowest lying triplet of **4** has been calculated at the UHF, projected UHF (PUHF), UMP2, and projected UMP2 (PUMP2) levels of theory by utilizing the MP2/6-31G(d) geometry of the singlet ground state.

The following energies (in hartrees) have been obtained: **4**, -302.509 47 (RHF/3-21G//RHF/3-21G), -304.235 74 (RHF/6-31G(d)//RHF/6-31G(d)), -305.202 56 (MP2/6-31G(d)//MP2/6-31G(d)); **5**, -302.639 67 (RHF/3-21G//RHF/3-21G), -304.335 35 (RHF/6-31G(d)//RHF/6-31G(d)).

The following energies (first entry RHF/6-31G(d) value, second entry RMP2/6-31G(d)//RHF/6-31G(d) value, both in hartrees) have been calculated to determine the strain energy of **4**: ethylene, -78.031 72, -78.294 31; ethane, -79.228 75, -79.503 97; propene, -117.071 47, -117.454 72; cyclopropene, -115.823 05, -116.218 39; propane, -118.263 65, -118.673 96; isobutene, -156.110 67, -156.645 57; isobutane, -157.277 53, -157.825 38; acetone, -191.962 24, -192.540 87; cyclopentadienone, -266.482 59, -267.301 59.

The analysis of the electron density distribution has been carried out by using MP2 response densities in the way described elsewhere.[42]

The CNDO/S method by Del Bene and Jaffe[15] has been employed to calculate the UV-vis spectrum of **4** and **14a**.

Acknowledgment. Financial support was given by the Deutsche Forschungsgemeinschaft (Schwerpunktprogramm "Noncovalent Interactions"), the Fonds der Chemischen Industrie, and the National Science Foundation of Sweden. D.C. thanks the National Supercomputer Centrum, University of Linkoping, Sweden, for the generous allotment of computer time. We thank T. Sommerfeld, C. Milbredt, and D. Faulstich for their valuable aid in preparing compounds [^{18}O]**6** and **14a**.

Registry No. 4, 133985-05-4; **4**-d_4, 133985-09-8; [^{18}O]-**4**, 133985-10-1; **5**, 3225-37-4; **5**-d_4, 133985-08-7; **6**, 932-97-8; **6**-d_4, 113567-96-7; [^{18}O]-**6**, 133985-07-6; **14a**, 32264-58-7; p-$O_2NC_6H_4N_2^{\cdot+}BF_4^-$, 456-27-9; p-$O_2NC_6H_4{}^{18}OH$, 20168-37-0; p-$H_2NC_6H_4{}^{18}OH$·HCl, 133985-06-5.

(42) Kraka, E.; Gauss, J.; Cremer, D. *THEOCHEM*, in press.

Reactivity Patterns and Comparisons in Three Classes of Synthetic Copper-Dioxygen $\{Cu_2-O_2\}$ Complexes: Implication for Structure and Biological Relevance

Partha P. Paul, Zoltán Tyeklár, Richard R. Jacobson, and Kenneth D. Karlin*

Contribution from the Departments of Chemistry, The Johns Hopkins University, Baltimore, Maryland 21218, and State University of New York at Albany, Albany, New York 12222.
Received December 10, 1990

Abstract: We have recently characterized three classes of peroxodicopper(II) complexes, which are formed reversibly from the reaction of Cu(I) precursors (**1**-**3**) with O_2 at -80 °C in solution. Here, we detail and compare the reactivities of $[Cu_2(XYL-O-)(O_2)]^+$ (**4**, a phenoxo-bridged peroxodicopper(II) species having terminal $Cu-O_2$ coordination), $[\{Cu(TMPA)\}_2(O_2)]^{2+}$ (**5**, a trans μ-1,2-peroxo-bridged complex with a tetradentate ligand on each copper(II) atom), and $[Cu_2(N4)(O_2)]^{2+}$ (**6**, which contains a bridging peroxo moiety with tridentate groups at both copper atoms). Complexes **4** and **5** possess a basic or nulceophilic peroxo group, but **6** behaves differently, possessing a nonbasic or electrophilic peroxodicopper(II) moiety. Thus, reaction of PPh_3 with **4** and **5** readily causes the stoichiometric displacement of the bound O_2 ligad, producing $Cu(I)-PPh_3$ complexes. With **6**, slow but complete oxygen atom transfer occurs, giving triphenylphosphine oxide. Protonation (or acylation) reactions are particularly striking, as addition of HBF_4 or HPF_6 to **4** and **5** gives near-stoichiometric yields of H_2O_2 (from excess H^+; iodometric titration), but **6** is relatively insensitive to protons. Carbon dioxide reacts with **4** and **5** to give peroxycarbonato complexes at -80 °C, which decompose to carbonato compounds; **6** does not react with CO_2. All three complexes **4**-**6** react with sulfur dioxide to give sulfato products. Trityl cation (Ph_3C^+) reacts with all the complexes to give benzophenone, but the relative yields again support the notion that the peroxo group in **6** is a poorer nucleophile. 2,4-Di-*tert*-butylphenol acts as a protic acid toward **4** and **5**, but in the presence of **6**, hydrogen atom abstraction leads to oxidatively coupled biphenol products. The reactions of 4-X-C_6H_4MgBr (X = CH_3, F) with **4**-**6** produce mixtures of 4-X-C_6H_4OH and substituted biphenyls; product ratios again support the view that **6** is a better one-electron oxidant and electrophilic reagent. The relationship of the observed reactivity patterns and structures of **4**-**6** is discussed, and it suggested that the μ-η^2:η^2-binding proposed for **6** confers its unique reactivity. The relationship of the structure and reactivity of **6** to a related and previously described monooxygenase model system is discussed, as well as the relevance to the active site chemistry of copper proteins involved in O_2 utilization.

Introduction

Understanding the relationship between structure and reactivity is a fundamental problem and challenge in chemistry and biochemistry. In our own laboratory, attempts to elucidate the intrinsic coordination chemistry occurring at active sites of copper proteins involved in O_2 utilization have led to the discovery and characterization of three different classes of $\{Cu_2-O_2\}^{n+}$ complexes (n = 1 or 2).[1] It is of interest to determine if these species possess varying reactivity patterns and if any of them may possess particular structures or functions seen in the copper enzymes. This has been the purpose of the present investigation.

The chemistry of peroxometal complexes is of interest in a number of disciplines, including its application to organic oxidation processes in chemical or biochemical systems.[2,3] Iron- and

*To whom correspondence should be addressed at the Department of Chemistry, The Johns Hopkins University, Charles & 34th Streets, Balitmore, MD 21218.

(1) Tyeklár, Z.; Karlin, K. D. *Acc. Chem. Res.* **1989**, *22*, 241-248.

(2) (a) *Oxygen Complexes and Oxygen Activation by Transition Metals*; Martell, A. E., Sawyer, D. T., Eds.; Plenum: New York, 1988. (b) Mimoun, H. *Catal. Today* **1987**, *1*, 281-295. (c) Gubelmann, M. H.; Williams, A. F. *Struct. Bonding (Berlin)* **1983**, *55*, 1. (d) Sheldon, R. A.; Kochi, J. K. *Metal-Catalyzed Oxidations of Organic Compounds*; Academic Press: New York, 1981. (e) Mimoun, H. In *The Chemistry of Functional Groups, Peroxides*, Patai, S., Ed.; Wiley: New York, 1983; pp 463-482.

0002-7863/91/1513-5322$02.50/0